Contrib Mineral Petrol (2005) 148: 662–674
DOI 10.1007/s00410-004-0630-y

ORIGINAL PAPER

Rolf L. Romer · Yilin Xiao

Initial Pb–Sr(–Nd) isotopic heterogeneity in a single allanite–epidote crystal: implications of reaction history for the dating of minerals with low parent-to-daughter ratios

Received: 9 July 2004 / Accepted: 1 October 2004 / Published online: 16 November 2004

Abstract We analyzed 17 fragments from a zoned allanite–epidote crystal (ca 2.2 mm × 4.0 mm), which had formed during different prograde and retrograde stages of ultra high pressure (UHP) and amphibolite facies metamorphism (240–230 Ma, Sulu Belt, E China), for the isotopic composition of Pb, Nd, and Sr and contents of Pb, U, and Th, Sr and Rb, and Nd and Sm. Since most fragments had $^{238}U/^{204}Pb$ and $^{232}Th/^{204}Pb$ values less than 1, corrections for in situ Pb growth are small and uncertainties in the recalculation of the Pb isotopic compositions to 240 Ma are insignificant. The recalculated Pb falls on a linear trend in the $^{206}Pb/^{204}Pb$ vs $^{207}Pb/^{204}Pb$ diagram with the allanite defining the low-$^{206}Pb/^{204}Pb$ end (17.07) of this trend and the epidote defining its high-$^{206}Pb/^{204}Pb$ end (17.56). The recalculated data scatter in the $^{206}Pb/^{204}Pb$ vs $^{208}Pb/^{204}Pb$ diagram, which implies that the initial Pb isotopic variation reflects the involvement of at least three different Pb sources. The low $^{87}Rb/^{86}Sr$ values account for a change in $^{87}Sr/^{86}Sr$ by in situ ^{87}Sr growth of less than 0.0007, which implies that the isotopic heterogeneity of $^{87}Sr/^{86}Sr$ (0.70601–0.7200) is a primary feature. The Pb and Sr isotope data unequivocally demonstrate that contributions from different precursor minerals result in initial isotopic heterogeneity in the metamorphic reaction product. It is likely that such an initial isotopic heterogeneity also exists for Nd, but it could not be resolved in the present study. Initially heterogeneous Pb and Sr isotope compositions imply that age differences between core and rim of large crystals may result in the determination of highly arbitrary geological rates, especially for minerals with relatively low parent-to-daughter ratios.

Editorial Responsibility: J. Hoefs

R. L. Romer (✉)
GeoForschungsZentrum Potsdam,
Telegrafenberg, 14473 Potsdam, Germany
E-mail: romer@gfz-potsdam.de
Tel.: +49-331-288-1405
Fax: +49-331-288-1474

Y. Xiao
Geowissenschaftliches Zentrum der Universität Gottingen,
Goldschmittstrasse 1, 37077 Göttingen, Germany

Introduction

Dating different phases of metamorphic development has traditionally faced two kinds of problems: (1) The minerals used for dating are minor constituents of the rock (e.g., zircon, monazite, xenotime) and they are in many cases difficult to relate to the texture or the metamorphic reaction used to constrain *P* and *T*. (2) Some texture-forming minerals are believed to have open isotopic systems at high temperature, implying that their age may not necessarily date the time of crystallization, but a later time when: (1) the temperature had fallen below the temperature of isotopic closure or (2) recrystallization driven by deformation and fluids had stopped. To avoid these potential ambiguities, the focus of dating had to be shifted from minerals of established geochonological applicability, such as zircon, monazite, xenotime, muscovite, and biotite, to minerals that are part of the mineral assemblages used to define *P–T* or that are part of the texture used to derive the deformation history of the rock. This shift resulted in the evaluation of garnet, rutile, staurolite, and vesuvianite (e.g., Mezger et al. 1989a, b; Romer 1992; Frei et al. 1995, 1997) as U–Pb geochronometers, the "rediscovery" of titanite for U–Pb dating (e.g., Tilton and Grünenfelder 1968; Schärer et al. 1994; Romer and Nisca 1995; Frost et al. 2001), and changes in the analytical approach. For instance, the dating of core and rim of the same crystal was used to derive rates of crystal growth, and by linking changes in the chemical composition of the dated minerals to prevailing pressure and temperature conditions as well as by using textural information (e.g., inclusion trails, pressure shadows), to determine rates of crystal growth and rock deformation, rates of burial and

exhumation, and rates of heating and cooling, respectively (Christensen et al. 1989, 1994; Stosch and Lugmair 1990; Mezger et al. 1989b; Vance and O'Nions 1990, 1992; Burton and O'Nions 1991; Vance and Harris 1999). Furthermore, the use of minerals that formed during different stages of a metamorphic evolution allowed to date different points along the loop and to extract information about heat and mass transfer in subduction systems from the shape–time relation of the loop (Barr and Dahlen 1989; Dahlen and Barr 1989). Similarly, major element zoning patterns and trace-element fingerprints may link the dated mineral to a particular reaction and, thus, indirectly to pressure, temperature, and deformation conditions in the rock (e.g., Möller et al. 2003; Nyström and Kriegsman 2003; Whitehouse 2003).

The basic assumption of all these studies was that isotopic differences are solely a function of age, that is, the dated minerals initially all had the same initial isotopic composition of the daughter element. Indications that this might not always be the case originate from an increasing number of studies yielding negative Sm–Nd isochron ages for high-grade rocks from young orogens ("futurechrons"; e.g., Jagoutz 1995; Thoeni 2002) and Sm–Nd garnet ages for high-grade rocks that were apparently younger than the age of low-grade rocks in the same area (cf. Romer and Smeds 1996; Page et al. 1996). For old rocks, anomalously young Sm–Nd garnet isochron ages have been interpreted as evidence for very slow cooling of granulite-facies rocks (e.g., Mezger et al. 1992; Burton et al. 1995) and temperatures of isotopic closure as low as 600°C for the Sm–Nd system in cm-sized garnet crystals and possibly even lower in smaller crystals (e.g., Humphries and Cliff 1982; Mezger et al. 1992; Burton et al. 1995; Johansson et al. 1991; Wang et al. 1998). This, however, was difficult to reconcile with trace-element zonation pattern on the micron-scale preserved in high temperature garnet (DeWolf et al. 1996; O'Brien 1997). The anomalous behavior of the Sm–Nd system in garnet was explained by the presence of monazite, allanite, and/or zircon inclusions (e.g., Zhou and Hensen 1995; DeWolf et al. 1996 Vance et al. 1998) and by initial isotopic heterogeneity as an effect of reaction history (Jagoutz 1995; Romer and Smeds 1996; Thoeni 2002). The recognition of the influence of trace minerals on the Sm–Nd budget of garnet eventually led to the development of a H_2SO_4-leaching scheme to remove monazite inclusions (Anczkiewicz and Thirlwall 2003). Anomalous ages were also documented for titanite and allanite that show apparent inheritance (Romer and Rötzler 2001, 2003; Romer and Siegesmund 2003; Rötzler et al., in press). The ages presented for these examples are older than expected from the regional context of the samples and geochronologic information available from the region. The older U–Pb ages are interpreted to reflect incorporation of radiogenic Pb from a precursor phase of the metamorphic assemblage and absence of isotopic homogeneity at small scale in melts that have been modified by the assimilation of U- and Th-rich minerals (with radiogenic Pb) from the wall rocks, respectively.

We present U–Th–Pb, Sm–Nd, and Rb–Sr isotope data from a single allanite–epidote crystal that has been subject to ultra high pressure (UHP) metamorphism to show that the initial isotopic compositions of Pb, Nd, and Sr were initially heterogeneous. The allanite-core of the crystal grew prograde near metamorphic peak conditions. A series of chemically distinct overgrowth zones of epidote formed during peak conditions and exhumation. Thus, this allanite–epidote crystal records a large segment of the metamorphic loop of the UHP rocks from the Sulu orogenic belt. We consider the growth of the investigated allanite–epidote crystal during both prograde and retrograde stages of the P–T path to represent a good analogue to the garnet crystals used to constrain the metamorphic evolution of other high-grade areas and to derive rates of deformation and change in P and T.

The optimal sample

For the documentation of initial isotopic heterogeneity, the optimal phase should have low parent-to-daughter (P/D) ratios to make post-crystallization daughter growth insignificant in comparison to the initial isotopic heterogeneity. Furthermore, the mineral should have sufficiently high contents of Pb, Nd, and Sr to determine precisely and accurately the initial isotopic composition of these elements even from small fragments of a single crystal.

Allanite—and to some extent also epidote—are phases with high contents of LREE and Sr, as well as low Sm/Nd and small Rb contents. Allanite typically has a few thousand parts per million (ppm) up to 1.5 wt% Th, up to several thousand ppm U, and up to several hundred ppm Pb (Barth et al. 1989, 1994; von Blankenburg 1992; Poitrasson 2002; Romer and Siegesmund 2003; Oberli et al. 2004; Gieré and Sorensen 2004). Thus, it should be generally suitable for determining initial Nd and Sr isotopic compositions, whereas Pb is commonly sufficiently radiogenic to permit U–Th–Pb dating (Barth et al. 1989, 1994; von Blankenburg 1992; Romer and Siegesmund 2003). Allanite from precursor rocks that are markedly depleted in U and Th, however, may have low U and Th contents, which would allow also for the Pb to remain unradiogenic and to preserve initial isotopic heterogeneity. Earlier work (e.g., Franz et al. 2001; Xu et al. 2002; Zhang and Sun 2002; Li et al. 2003) suggests that the entire Dabie Shan and Sulu region is characterized by unradiogenic Pb, whose retarded signature implies that these rocks or their precursors had experienced U (and Th) depletion more than 1.8 Ga ago.

In the Sulu–Dabie Shan orogenic belt large volumes of continental crust that had been subducted to a depth greater than 100 km are exposed at the present surface (e.g., Okay et al. 1989; Xu et al. 1992; Liu et al. 2002). Although the metamorphic evolution of the different

units in the Dabie Shan and Sulu belts differ in path, peak conditions, and timing, there is a broad consensus that UHP units evolved from prograde pre-eclogite-facies metamorphism at < 17 kbar and < 700°C through peak metamorphic conditions of > 30 kbar and 800–900°C to a retrograde metamorphic stage at 9–13 kbar and 600–700°C (e.g., Xiao et al. 1995, 2002; Zhang and Liou 1998). U–Pb dating indicates that UHP conditions in the Dabie Shan and Sulu belts occurred at 240–230 Ma, whereas retrogression under amphibolite-facies conditions may have been as late as 210 (Ames et al. 1993; Li et al. 1993, 2000; Liu et al. 2004).

Sample description

The investigated sample comes from a UHP eclogite collected from a depth of 1,065 m of the Chinese continental Scientific Drilling (CCSD) main hole at Donghai, Sulu belt (for details of the CCSD see Xu et al. 1998). The allanite-bearing eclogite originates from about 30 m thick eclogite body enclosed in paragneiss. The handspecimen is relatively fresh and consists of garnet (~45%), omphacite (~35%), phengite (~12%), allanite–epidote (~5%), rutile (~2%), with minor ilmenite, apatite, and zircon. In rare cases, omphacite is replaced at the margin by a thin veneer of amphibole–plagioclase symplectite. Allanite-epidote porphyroblasts in the eclogite coexist with coarse-grained garnet and omphacite. In thin sections, allanite cores appear as darker areas in the epidote.

The studied allanite–epidote crystal is about 2.2 mm×4.0 mm. On back-scattered electron (BSE) images, the crystal displays a series of chemically distinct zones that reflect expitaxial overgrowth of different types of epidote on the central allanite (Fig. 1a). The regular pattern is only disturbed by inclusions and slight alteration along a few fractures that penetrate the transition zone (Fig. 1), but do not cut across the core. The allanite core is LREE-enriched with Ce_2O_3 up to 5.07 wt%, La_2O_3 up to 2.88 wt%, and abundant other REE elements ($Nd_2O_3 = 1.66\%$, $Pr_2O_3 = 0.38\%$, $Sm_2O_3 = 0.27\%$; Y.L. Xiao et al., unpublished data). The ThO_2 content is locally as high as 1.67 wt%.

The distribution of mineral inclusions suggests that the allanite–epidote crystal formed at a wide range of *P–T* conditions, including prograde, peak UHP, and retrograde amphibolite-facies metamorphism (Fig. 1).

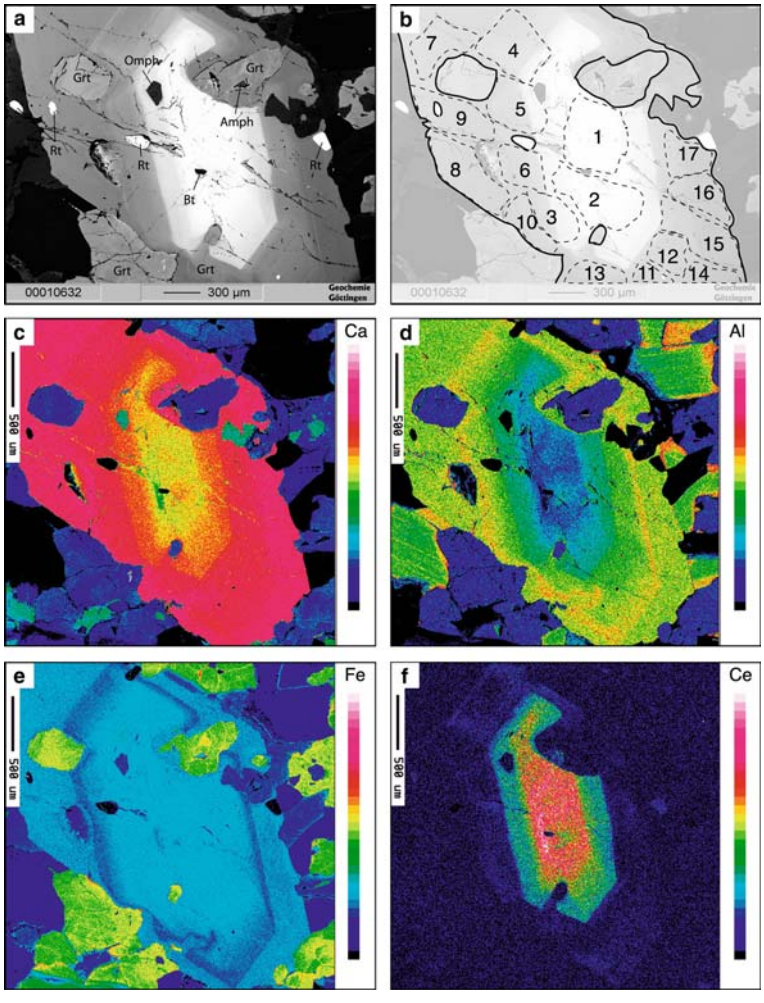

Fig. 1 Electron microprobe map of the analyzed allanite–epidote crystal. **a**. Back-scattered electron image. **b**. Drawing of the crystal showing the position of the individual fragments (1–17). **c–f**. Element map produced by rastering the sample at 1 µm steps. Color bar represents a linear scale.

Biotite inclusions in the very center of the allanite indicate that the core may have formed during prograde amphibolite-facies metamorphism. Inclusions of garnet, omphacite, and rutile occur in the transition zone between allanite and epidote, suggesting that this zone grew under eclogite-facies, probably even near peak (UHP) conditions (allanite is stable up to temperatures of 1,000°C and to pressures of at least 4.0 GPa, Hermann 2002). The outermost part of the porphyroblast contains biotite and amphibole inclusions, which indicates that epidote crystallized during retrogression under amphibolite-facies conditions. Thus, the porphyroblasts of allanite–epidote may have grown over a period of a few million years. The distribution of fluid inclusions in the grain also indicated that the porphyroblast formed under varying metamorphic conditions. Fluid inclusions in the allanite core are small and abundant, whereas those in the epidote rim are larger and less abundant. Fluid inclusions of the core have ice melting temperatures of −19.3 to −12.6°C, whereas those of the rim show ice melting temperatures of −13.1 to −6.8°C, indicating compositionally different fluid systems during their formation (Xiao et al., unpublished data).

Pb–Nd–Sr isotope systematics

Sample preparation

All analyzed fragments were derived from one single crystal that was characterized by element mapping using a polished thick section. The chemical zonation of the investigated allanite–epidote crystal is shown in Fig. 1. In a first step, the allanite–epidote crystal was freed from surrounding silicate minerals. Then, the sample was broken into 17 small fragments and the position of each fragment within the crystal was recorded (Fig. 1b). Each fragment was checked for inclusions, intergrowth with other phases, and homogeneous color. Impurities or parts with stronger or weaker greenish tint were removed (Fig. 2d).

Ion-exchange chromatography and loading for measurement followed standard procedures. Using the procedure described by Romer et al. (2004), Pb, Th, and U were purified on AG1-8X resin in 200 µl ion-exchange columns, collecting Th before eluting U. The Pb isotopic composition was determined on a Finnigan MAT262 mass-spectrometer by static multi-collection using Faraday collectors. The reported isotope ratios are corrected for contributions from tracer and blank Pb and by 0.1%/a.m.u. for mass fractionation as determined from the repeated measurement of Pb reference material NBS981. The reported Pb isotopic ratios are known better than 0.1% at the 2σ level. U was loaded with phosphoric acid and silica gel. It was analyzed as UO_2. Th was loaded with HNO_3 using a graphite-sandwich technique and analyzed as metal. Sr and Nd were separated and purified using ion-exchange chromatography as described in Romer et al. (2001). $^{87}Sr/^{86}Sr$ ratios were determined on a VG54-40 Sector mass-spectrometer using dynamic multi-collection in a triple-jump experiment. All ratios were normalized to $^{86}Sr/^{88}Sr = 0.1194$. Over the measurement period, Sr reference material NBS 987 gave a value of $^{87}Sr/^{86}Sr = 0.710256 \pm 9$ (2σ reproducibility, $n = 12$). $^{143}Nd/^{144}Nd$ ratios were obtained on a Finnigan MAT262 multi-collector mass-spectrometer using dynamic multi-collection in a double-jump experiment. All ratios were normalized to $^{146}Nd/^{144}Nd = 0.7219$. Nd reference material LaJolla gave a value of $^{143}Nd/^{144}Nd = 0.511852 \pm 5$ (2σ reproducibility, $n = 10$) over the measurement period. Analytical uncertainties for $^{87}Sr/^{86}Sr$ and $^{143}Nd/^{144}Nd$ are given at $2\sigma_m$ (standard error of the mean) level.

Results

The analytical results for Pb, Sr, and Nd isotopic determinations and U, Th, Pb, Rb, Sr, Sm, and Nd concentrations are shown in Table 1. Note that not all fragments were analyzed for Sr and Nd and that some fragments had too low contents of Sr and Nd to determine reliably the isotopic composition of these elements.

Lead

The isotopic compositions of Pb define three major groups in the $^{206}Pb/^{204}Pb$ vs $^{207}Pb/^{204}Pb$ and $^{206}Pb/^{204}Pb$ vs $^{208}Pb/^{204}Pb$ diagram: (1) One group (samples 1 and 2) is characterized by high contents of Pb, U, and Th, intermediate measured $^{206}Pb/^{204}Pb$ values and high $^{208}Pb/^{204}Pb$ values. The high Th contents and Th/U values are characteristic for allanite. (2) The second group of three samples (3, 4, and 5; Table 1) has low measured $^{206}Pb/^{204}Pb$, high Pb contents, and intermediate U and Th contents. (3) The third group includes 12 samples of epidote (6–17; Table 1). It is characterized by high Pb, low U (4–18 ppm), and a broad range (0.14–33 ppm) of Th contents and relatively high measured $^{206}Pb/^{204}Pb$ ratios (17.49–17.57).

The initial Pb isotopic composition of all fragments is corrected for 240 Ma of in situ Pb growth (Table 1, Fig. 2). The largest correction was obtained for the two allanite fragments that yield unradiogenic recalculated Pb isotopic composition with $^{206}Pb/^{204}Pb \approx 17.08$. The three samples of group (2) had only minor reductions of their $^{206}Pb/^{204}Pb$ to 17.20–17.27 (Table 1), whereas the epidote samples of group (3) had a neglishible shift in their $^{206}Pb/^{204}Pb$ ratios by in situ Pb growth. The two epidote samples with the highest $^{206}Pb/^{204}Pb$ (samples 16 and 17, Table 1) also had a slightly larger shift of $^{208}Pb/^{204}Pb$ than the other epidote samples (Fig. 2c). The initial Pb isotopic composition of all fragments falls approximately on a two-component mixing trend in the $^{206}Pb/^{204}Pb$ vs $^{207}Pb/^{204}Pb$ diagram. Most samples also fall on a two-component mixing line in the $^{206}Pb/^{204}Pb$ vs $^{208}Pb/^{204}Pb$ diagram. The two epidote samples with the largest correction in $^{208}Pb/^{204}Pb$ (samples 16 and 17,

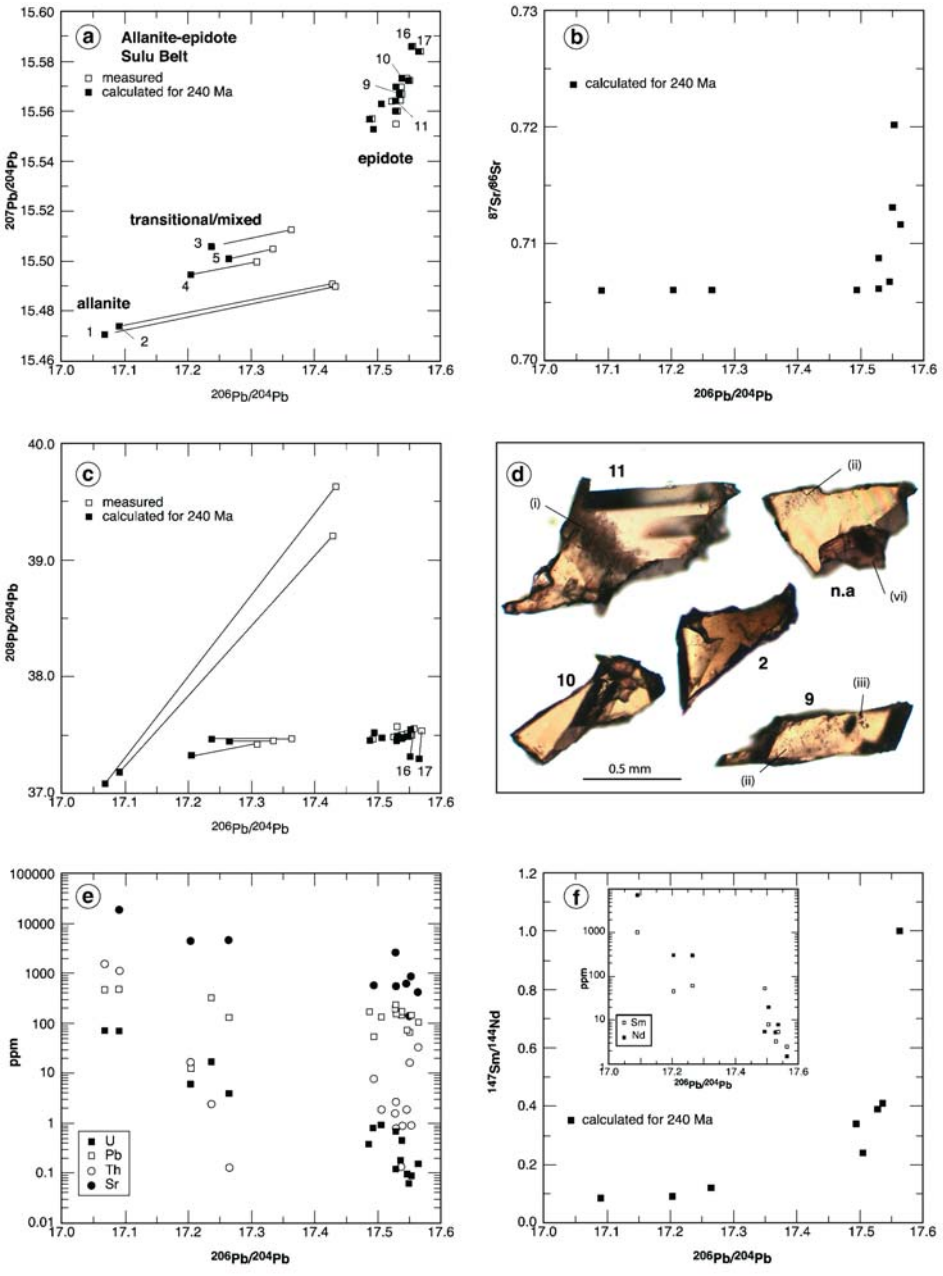

Fig. 2 Samples and results. **a** Measured and recalculated $^{206}Pb/^{204}Pb$ and $^{207}Pb/^{204}Pb$ values. Note the systematic variation in the Pb isotopic composition from allanite to epidote. Numbers correspond to sample numbers in Table 1 and fragments in d. **b** $^{87}Sr/^{86}Sr$ ratios recalculated to 240 Ma. **c** Measured and recalculated $^{206}Pb/^{204}Pb$ and $^{208}Pb/^{204}Pb$ values. **d** Sample fragments. Individual fragments were crushed and further purified before analysis. (1) irregular rim with needles between allanite and epidote; (2) trail of fluid inclusions; (3) solid inclusions; (4) garnet; Numbers correspond to samples in Table 1. *na* = fragment not analyzed, consists in part of garnet. **e** Concentration profiles as a function of initial $^{206}Pb/^{204}Pb$ isotopic composition. Note the sharp decrease of Th contents (*line*) relative to U, Pb, and Sr. **f** $^{147}Sm/^{144}Nd$ and Nd and Sm contents as a function of recalculated $^{206}Pb/^{204}Pb$ isotopic composition.

Table 1), however, fall below this mixing trend indicating the involvement of a third component. The two allanite samples (1 and 2, Table 1), which are texturally oldest, have the least radiogenic Pb, whereas the samples from the younger epidote (samples 6–17, Table 1) have the most radiogenic Pb. Two possible explanations for this systematic variation are: (1) The time difference between different stages of metamorphism that are related to the growth of allanite and epidote allowed the Pb isotopic composition to evolve from the composition found in allanite to the more radiogenic composition found in epidote. The apparent initial isotopic heterogeneity is due to the in situ Pb growth in the precursor. For a time difference of about 10 Ma between the growth of allanite and the growth of the youngest epidote, the precursor minerals would have to have an average μ value of 290 to account for a difference in $^{206}Pb/^{204}Pb$ of 0.47 between the least radiogenic (allanite) and the most radiogenic samples (epidote). This value is distinctly higher than generally known for crustal rocks (Stacey and Kramers 1975; Zartman and Doe 1981) and than found in the analyzed allanite (9.59; Table 1), which is a phase known to accept considerable amounts of U and typically to show high μ values (e.g., Barth et al. 1989, 1994; Oberli et al. 2004). Furthermore, the general unradiogenic nature of Sulu–Dabie Shan Pb in combination with such a high short-lived μ in the precursor phases would imply that a U-depleted rock suddenly increased its μ value (by addition of U or by marked loss of Pb) only to reduce it again during the low-*P* segment of the metamorphic

Table 1 Sr, Nd, and Pb isotope data from a single, zoned c. 240 Ma old allanite–epidote crystal (Sulu UHP belt, eastern China)

Sample[a]	Weight (mg) [a]	Rb (ppm)	Sr (ppm)	$^{87}Sr/^{86}Sr$[b]	$^{87}Sr(T)/^{86}Sr$[c]	Nd (ppm)	Sm (ppm)	$^{143}Nd^{144}Nd$[b]	$^{147}Sm/^{144}Nd$[b]	εNd[c] (T)	Weight (mg) [a]	$^{206}Pb/^{204}Pb$[d]	$^{207}Pb/^{204}Pb$[d]	$^{208}Pb/^{204}Pb$[d]	U (ppm)	Th (ppm)	Pb (ppm)	μ[e]	ω[e]	$^{206}Pb/^{204}Pb$[f]	$^{207}Pb/^{204}Pb$[f]	$^{208}Pb/^{204}Pb$[f]
1. allanite											0.048	17.432	15.490	39.634	73.1	1570	485	9.59	213.5	17.068	15.471	37.084
2. allanite	0.050	1.1	18300	0.706012 ± 14	0.70601	7330	1040	0.511976 ± 5	0.0858	−9.5	0.044	17.429	15.491	39.209	68.1	1110	484	8.90	169.2	17.091	15.474	37.187
3. trans.	0.202	7.7	4580	0.706049 ± 11	0.70603	309.4	62	0.512025 ± 7	0.12*	−9.6	0.112	17.334	15.505	37.452	4.00	0.13	134	1.83	0.1	17.265	15.501	37.451
4. trans.	0.160	28	4470	0.706087 ± 11	0.70603	316.3	46.7	0.512060 ± 7	0.0893	−8.0	0.142	17.308	15.500	37.421	5.95	17.	13	2.75	8.2	17.204	15.495	37.324
5. trans.											0.049	17.364	15.513	37.470	17.6	2.5	323	3.37	0.5	17.236	15.506	37.464
6. epidote	0.179	0.4	589	0.706059 ± 62	0.70605	5.5	54.3	0.512032 ± 8	0.34*	−16	0.127	17.528	15.555	37.565	0.822	7.6	55.7	0.91	5.0	17.493	15.553	37.505
7. epidote	0.042			–				–			0.055	17.535	15.564	37.463	0.667	1.6	201	0.21	0.5	17.527	15.564	37.457
8. epidote											0.066	17.491	15.557	37.457	0.390	0.39	171	0.14	0.1	17.486	15.557	37.455
9. epidote	0.039	5.0	2630	0.706182 ± 41	0.70616			–			0.051	17.536	15.570	37.488	0.668	2.7	233	0.18	0.8	17.529	15.570	37.479
10. epidote	0.372	4.8	632	0.70678 ± 14	0.7067			–			0.144	17.549	15.573	37.499	0.098	1.9	71.3	0.09	1.7	17.546	15.573	37.479
11. epidote	0.233			–		20.3	8	0.512196 ± 22	0.24*	−10	0.085	17.523	15.564	37.476	0.950	1.9	133	0.44	0.9	17.506	15.563	37.465
12. epidote											0.088	17.545	15.573	37.500	0.465	0.89	152	0.19	0.4	17.538	15.573	37.496
13. epidote	0.057	22	874	0.72021 ± 64	0.7200			–			0.085	17.555	15.586	37.538	0.090	0.92	139	0.04	0.3	17.553	15.586	37.535
14. epidote	0.217	4	568	0.70878 ± 45	0.7087	5.4	3.4	0.51305 ± 15	0.39*	+2.1	0.068	17.530	15.560	37.452	0.123	0.78	161	0.05	0.3	17.528	15.560	37.448
15. epidote	0.059			–		8.1	5.5	0.512554 ± 85	0.41*	−8.2	0.062	17.538	15.567	37.474	0.177	0.14	169	0.06	0.0	17.536	15.567	37.473
16. epidote	0.324	10	141	0.71320 ± 63	0.7125			–			0.156	17.552	15.572	37.492	0.064	16	67.9	0.06	15.2	17.550	15.572	37.310
17. epidote	0.110	8.3	429	0.71168 ± 80	0.7115	1.5	2.5	–	1. **		0.108	17.567	15.584	37.527	0.154	33	106	0.09	20.5	17.564	15.584	37.282

[a]All fragments were rinsed in 7 N HNO_3 and distilled water before weighing and dissolution overnight in 52% HF at 160°C on the hot plate. The digested samples were dried and redissolved in 6N HCl. All samples with a weight less than 0.068 mg were spiked with a mixed $^{205}Pb-^{235}U$ and a ^{229}Th isotopic tracer. The other samples were split by weight. One aliquot was used for the U-Th-Pb investigation, the other aliquot was split ~9:1, the smaller fraction being spiked with a mixed $^{149}Sm-^{150}Nd$ and a mixed $^{84}Sr-^{85}Rb$ tracer. This second aliquot was made to avoid large spike correction that may occur in samples with unexpectedly low contents of Nd and Sr. Spiked fragments correspond to 0.025 to 0.004 mg of epidote-allanite. Sr and Nd were separated and purified using ion-exchange chromatography as described in Romer et al. (2001), Pb, Th, and U were purified using the procedure described in Romer et al. (subm.) on 200 µl ion-exchange columns, collecting Th before eluting U. Weights given in the table correspond to the alliquots used for Rb, Sr, Sm, and Nd and for Th, U, and Pb analysis, respectively. Trans. refers to samples dominated by the transitional zone between the allanite core and the epidote rim

[b] $^{87}Sr/^{86}Sr$ ratios were determined on a VG54-40 Sector mass-spectrometer using dynamic multi-collection in a tripple-jump experiment. All ratios were normalized to $^{86}Sr/^{88}Sr = 0.1194$. $^{143}Nd/^{144}Nd$ were obtained on a Finnigan MAT262 multi-collector mass-spectrometer using dynamic multicollection. All ratios were normalized to $^{146}Nd/^{144}Nd = 0.7219$. Analytical uncertainties are given at $2\sigma_m$ (standard error of the mean) level

[c] $^{87}Sr/^{86}Sr$ (T), $^{143}Nd/^{144}Nd$(T), and ε_{Nd} (T) were calculated for 240 Ma, using $\lambda^{87}Rb = 1.42E\text{-}11\ y^{-1}$ and $\lambda^{147}Sm = 6.54E\text{-}12\ y^{-1}$, $(^{147}Sm/^{144}Nd)^0_{CHUR} = 0.1967$, and $(^{143}Nd/^{144}Nd)^0_{CHUR} = 0.512638$, respectively. The concentrations of Rb, Sr, Nd, and Sm were determined by isotope dilution. Because of the small sample size and the low contents of Nd and Sm, some ID runs were overspiked (marked with * and **, respectively), and the values $^{87}Rb/^{86}Sr$ and $^{147}Sm/^{144}Nd$ of these samples are not known better than 5% to 10%

[d]Lead isotope analyses data corrected for mass discrimination with 0.1%/A.M.U., 15 pg Pb blank, and tracer contribution. Reproducibility at 2-sigma level is better than 0.1%

[e] $\mu = {}^{238}U/{}^{204}Pb$; $\omega = {}^{232}Th/{}^{204}Pb$

[f]Lead isotope analyses data recalculated to 240 Ma using the Pb, U, and Th concentration data obtained by isotope dilution, the measured isotope ratios, and the decay constants of Le Roux and Glendenin (1963) and Jaffey et al. (1971) recommended by IUGS (Steiger and Jäger 1977). Concentration ratios are known better than 0.5% (1–3% for samples with low U contents)

path. Therefore, it is unlikely that the contrast in initial Pb isotopic composition between allanite and epidote originated from in situ Pb growth in the precursors during the short period between the growth of allanite and epidote. (2) The initial Pb isotopic heterogeneity reflects the involvement of different precursor minerals at different stages of the metamorphic evolution. The Pb line through the initial Pb isotopic composition (i.e., $t = 240$ Ma) of the allanite–epidote samples in the $^{206}Pb/^{204}Pb$ vs $^{207}Pb/^{204}Pb$ diagram has a $^{207}Pb/^{206}Pb$ slope of ~0.2, implying an age of ~2,700 Ma for the precursor minerals (for a single-stage pre-UHP history of the magmatic protolith).

Strontium

All analyzed fragments have high Sr contents, ranging from 18,300 ppm in allanite to 140–870 ppm in epidote. In contrast, Rb contents are low, falling into the range from 0.4 to 28 ppm (Table 1). Although samples with low Sr contents have higher Rb, the overall correction for in situ Sr growth is insignificant. It ranges from less than 1 in the fifth digit for allanite to as much as 7 in the fourth digit for one epidote sample (Table 1). Differences in the Sr isotopic composition of individual allanite–epidote samples, however, are much larger. The least radiogenic initial Sr is found in allanite, the samples from the transitional zone (0.70601–0.70616), and two epidote samples. Five other epidote samples have more radiogenic initial $^{87}Sr/^{86}Sr$ with values as high as 0.7200. Radiogenic Sr is only found in samples with Sr contents below 1,000 ppm (Table 1). The broad range of Sr isotopic compositions in epidote is likely to reflect contrasting precursor phases rather than in situ Sr growth. For instance, a 1.8 Ga old amphibole with a $^{87}Rb/^{86}Sr$ value of 0.625 would have sufficiently radiogenic Sr to account for the most radiogenic Sr in the analyzed epidote fragments. The alternative interpretation that the $^{87}Sr/^{86}Sr$ range of 0.014 was produced in situ in less than 10 Ma would require precursor minerals with $^{87}Rb/^{86}Sr$ values larger than 100. Such high values are common for biotite and phlogopite, which, however, have relatively low Sr contents. The 140–870 ppm of Sr in epidote would require large amounts of such short-lived precursor minerals, which is unlikely in the investigated eclogite.

Neodymium

Allanite and epidote commonly have REE patterns with a pronounced LREE-enrichment relative to the HREE (e.g., Gromet and Silver 1983; Bea 1996; Gieré and Sorensen 2004). The analyzed samples range in $^{147}Sm/^{144}Nd$ from 0.0858 to ~1 (Table 1). Low $^{147}Sm/^{144}Nd$ values are found in REE-rich early-formed allanite, whereas the high $^{147}Sm/^{144}Nd$ values are associated with late-formed epidote. The contents of Nd differ by several orders of magnitude between early allanite (7,300 ppm Nd) and late epidote (1–10 ppm Nd) and they correlate with the Pb isotopic composition (Fig. 2f). The shift to high $^{147}Sm/^{144}Nd$ in late epidote may reflect depletion of the local environment in LREE during the crystallization of the LREE-rich allanite. The residue had a high $^{147}Sm/^{144}Nd$ and late epidote eventually inherited this $^{147}Sm/^{144}Nd$ signature. Recalculation to 240 Ma yields $\epsilon Nd_{(T)}$ values in the range of −8 to −10 (Table 1), which would suggest that the host-rock of the epidote–allanite had a long crustal residence before being metamorphosed under UHP conditions. The heterogeneity in initial Nd isotopic composition is not so well documented as the biggest variation is shown by two samples (6 and 14, Table 1) that have very low Nd contents and extremely high $^{147}Sm/^{144}Nd$ values. Nonetheless, the $^{143}Nd/^{144}Nd$ values of these two samples is reconcilable with a dominant derivation of Nd from an old high $^{147}Sm/^{144}Nd$ mineral (sample 14), such as garnet, and from an old low $^{147}Sm/^{144}Nd$-mineral (sample 6), such as feldspar, respectively.

Reaction history

The change in isotopic and elemental signatures during growth of allanite and epidote, reflects initial growth of allanite from precursor minerals characterized by low $^{206}Pb/^{204}Pb$ and $^{87}Sr/^{86}Sr$ values, high contents of Th, Pb, Sr, Nd, and Sm, intermediate contents of U and Pb, and low contents of Rb, and later growth of epidote from a source characterized by high $^{206}Pb/^{204}Pb$ and high $^{87}Sr/^{86}Sr$ values, low contents of Th, U, Rb, Nd, and Sm, intermediate contents of Sr and Pb, and high $^{147}Sm/^{144}Nd$. All samples define a linear trend in the $^{206}Pb/^{204}Pb$ vs $^{207}Pb/^{204}Pb$ diagram (Fig. 2a). This trend can be interpreted as two-component mixing at ca 240 Ma of Pb derived from a ca 2,700 Ma old mineral assemblage. Because of the highly correlated nature of $^{206}Pb/^{204}Pb$ and $^{207}Pb/^{204}Pb$, such a two-component mixing line does not require two distinct end-members. Instead, the trend can also be obtained by incomplete mixing of Pb from a wide range of sources (e.g., different precursor minerals) that have the same age and initially had the same Pb isotopic composition (cf. Faure 1986; Romer and Wright 1993; Romer 2001). The presence of several mineralogically different sources is most clearly demonstrated by the scatter in the $^{206}Pb/^{204}Pb$–$^{208}Pb/^{204}Pb$ diagram that is due to different Th/U ratios in the various precursor minerals. The shift from one precursor signature to another precursor signature does not occur for all isotope systems in parallel, which reflects: (1) the involvement of several precursor phases, (2) the importance of partitioning of the various elements between precursor and product phases and among the various product phases, and (3) the local depletion of elements with high K_D in the source.

Using the systematic variation of the Pb isotopic composition from allanite to epidote as a rough measure for source evolution and plotting the concentrations of U, Th, Pb, Sr, Sm, and Nd against the Pb isotopic

composition (Fig. 2e and f), we observed the following systematic variations: (1) The Sr contents are especially high in allanite and drop by about two orders of magnitude towards epidote. The Sr isotopic composition shows little variation from allanite through the transitional zone to some epidote samples. The large range in Sr isotopic composition among the epidote samples (Fig. 2b), however, suggests that the Sr budget of epidote is not controlled by the same reservoir that dominated the Sr isotopic compositions of allanite and early epidote. (2) The Pb contents drop slightly from allanite to epidote (Fig. 2e). There is only one sample from the transitional zone with markedly lower Pb contents. (3) The contents of Th drop sharply from the allanite core to the transitional zone, which may indicate that allanite crystallization strongly depleted Th in the source. The fragments of late epidote (samples 16 and 17) with more radiogenic initial Pb have more Th than samples from the transitional zone, indicating that Th was again available during growth of this epidote, when a different silicate source (also reflected in high $^{87}Sr/^{86}Sr$ values) was consumed. (4) Nd and Sm contents drop systematically with increasing $^{206}Pb/^{204}Pb_{init}$ values (Fig. 2f, inset), whereas $^{147}Sm/^{144}Nd$ values increase from 0.085–0.089 in allanite to 0.4–1 in late epidote. The investigated epidote has lower Nd and Sm contents (Nd: 1.5–20.3 ppm; Sm: 2.5–8 ppm) than typically observed in epidote from allanite-free rocks (e.g., Frei et al. 2004). It is likely that epidote incorporated most of the little REE available after allanite crystallization, which would imply that the high $^{147}Sm/^{144}Nd$ values reflect the depletion of REE and especially LREE during allanite crystallization. These variations suggest that the source was characterized by high contents of Sr, Pb, and REE. Furthermore, the source is likely to have been enriched in U and Th relative to the whole-rock sample.

Allanite in the Sulu Belt could have formed at the expense of either monazite or zoisite. Monazite has been documented to decompose according to the reaction monazite + biotite + plagioclase + H_2O = allanite + apatite + epidote + quartz and monazite + calcic plagioclase + H_2O = allanite + apatite + thorite + Ca-poorer plagioclase (e.g., Finger et al. 1998; Parrish 2001; Grapes et al. 2002). This mineral would be an ideal source for the high contents of Th, Nd, and Sm in allanite. The following points, however, argue against a monazite precursor. Firstly, the formation of allanite at the expense of monazite should result–depending on P and T conditions and rock chemistry – in the formation of apatite (e.g., Finger et al. 1998; Grapes et al. 2002). There is no apatite associated with allanite. Furthermore, no relicts of monazite have been observed. The Pb isotopes provide the strongest argument against a monazite precursor. Monazite has high Th contents and typically also high $^{232}Th/^{204}Pb$ values. Therefore, it should develop high $^{208}Pb/^{204}Pb$ values with time. The initial Pb isotopic composition of allanite, however, is low in $^{208}Pb/^{204}Pb$. Thus, it is unlikely that allanite derived its Pb from a monazite precursor.

The decomposition of zoisite under prograde UHP conditions may follow a reaction of the type zoisite + amphibole/biotite = clinopyroxene + kyanite + allanite + fluid/melt (Hermann 2002). Zoisite can carry significant amounts of Sr and REE (Nagasaki and Enami 1998; Frei et al. 2004), high contents of Pb, and variable contents of Th (0.08–130 ppm; Frei et al. 2004). The formation of allanite from zoisite is supported by the presence of biotite inclusions in allanite and amphibole relicts in garnet (Fig. 1a). Since zoisite has lower Th, U, and REE contents than allanite, these elements are rapidly depleted during the formation of allanite and could explain their sharp decrease from allanite to the transition zone. The Pb isotopic composition indicates that Pb is not solely derived from zoisite, but may be derived to a progressively higher extent from the consumed Mg-silicate. In contrast, the essentially constant $^{87}Sr/^{86}Sr$ ratio in the range of 0.706012–0.706182 indicates that the Sr content of zoisite buffered the Sr isotopic composition of the source.

The formation of allanite from zoisite may result from a solid state reaction or crystallization from a melt. A solid state reaction would require that the chemical composition of precursor zoisite was continuously changed, that is zoisite became depleted in elements that strongly fraactionate into allanite (Th, Nd, Sm, and possibly Sr) and enriched in elements that did not fractionate into allanite. Crystallization of allanite from a very small and local volume of melt, which is the preferred explanation, would result in the depletion of Th, Nd, and Sm in the melt. Thus, the development of a transition zone between allanite and epidote may reflect the depletion of some elements in the source rather than a change in precursor. The homogeneous isotopic compositions of Sr and Nd in conjunction with the depletion of Th, Sm, and Nd in allanite and some epidote fragments indicate that the budget of these elements during early crystallization of allanite and epidote was dominated by the zoisite source, which is considered to have relatively high contents of these elements. The slight shift of the Pb isotopic composition and the distinct shift of the Sr isotopic composition, which are uncoupled from each other, reflect the increasingly higher response to input of Pb and Sr from other silicates. The effect of this additional Pb and Sr is higher as the zoisite-derived reservoir becomes increasingly depleted.

Orogens and distorted time scales

Despite the importance of dating geological rates (e.g., deformation, heating, and cooling) for the understanding of orogenic processes, isotopic dating dominantly relied on the assumptions of (1) a homogeneous initial composition of the daughter element (e.g., Pb, Sr, and Nd) and (2) mineral-specific temperature ranges for isotopic closure. There is increasing geological, petrological, and mineralogical evidence to suggest that the

above assumptions may not always apply, which eventually results in distorted time-scales.

The large range of isotopic ages obtained for many Archaean and Palaeoproterozoic high-grade units has been used to argue that these units experienced very slow cooling (1–3°C/Ma) and exhumation rates (e.g., Mezger et al. 1992; Burton et al. 1995; Humphries and Cliff 1982). These slow cooling rates contrast with the fast rates of cooling and exhumation of metamorphically and tectonically comparable complexes, which typically are one order of magnitude higher (e.g., Duchène et al. 1997; Rubatto and Hermann 2001; Romer and Rötzler 2001; Rötzler et al. (2004). If this is true, the contrast in rates would imply that old orogens worked differently from young ones (or slowly cooling and slowly exhuming complexes are not yet available for sampling in young orogens). The slow rates in old high-grade rocks, however, may reflect ages from more than one orogenic loop (e.g., Kamber et al. 1995), in which case estimates of geological rates are highly arbitrary.

Detailed BSE imaging of garnet from the Western Gneiss Region (Norway) has shown that garnet in the ca 420–400 Ma old Caledonian UHP eclogites consist of a Grenvillian core (ca 960–980 Ma) and a very thin Caledonian veneer. The Grenvillian core formed under granulite-facies metamorphism. Thus, although garnet is an essential part of the Caledonian eclogite mineral assemblage, it had already formed during an earlier, entirely unrelated event (Erambert and Austrheim 1993). In other areas, such relict minerals may also be an integral part of later mineral assemblages. If the time difference between the two events is relatively small, the younger event may not be recognized as a separate event. Instead, it may be misinterpreted as retrograde stage of the first event.

During metamorphic reactions, both type and proportions of precursor minerals change. As these minerals have a wide range of parent-to-daughter element ratios, they have developed contrasting isotopic compositions of the daughter element with time. Thus, product minerals or different zones of a product mineral may have distinct initial isotopic compositions. If corrections for initial presence of a daughter element are made using a common isotopic composition, some samples may become too young or too old, that is the time difference between different minerals or core and rim of the same mineral may be too large, too small, or even inverted (e.g., Jagoutz 1995; Lanzirotti and Hanson 1995; Thoeni 2002). The effect of a heterogeneous initial isotopic composition becomes especially important if the initially incorporated daughter element is radiogenic (e.g., Romer 2001; Romer and Rötzler 2003).

Factors other than temperature may control isotopic closure. For instance, Villa (1998) and Glodny et al. (2003) argued that fluids, defect density, deformation, and recrystallization outweigh the effect of temperature. Equally important is whether the daughter element, which is supposed to be lost by volume diffusion from the mineral at temperatures exceeding the ''temperature of isotopic closure'', can be transported away from the mineral surface. For instance, phlogopite in ultramafic rocks of the Western Gneiss Region (Norway) that experienced Caledonian eclogite facies metamorphism yield Grenville ages (Kühn et al. 2000), which implies that the phlogopite had formed during the Grenville granulite metamorphism. During the Caledonian event, the rocks reached temperatures far above literature values for the isotopic closure temperature of phlogopite. However, as the metamorphic mineral paragenesis of this rock contained no phases that did accept strontium into its structure, the Rb–Sr systematics of the phlogopite remained undisturbed. Thus, minerals commonly thought to be highly susceptible to resetting of their isotopic clock may remain closed systems even at extreme temperatures depending on the neighboring minerals (Kramers et al. 1999; Kühn et al. 2000).

The reaction rates determined from laboratory experiments and from contact metamorphic aureoles differ from those determined on regionally metamorphosed rocks by several orders of magnitude (Baxter 2003). Among the possible reasons for this discrepancy, Baxter (2003) discusses the importance of intergranular transport and the availability of fluids, but leaves out the possibility of incorrect dating of mineral growth. Several of the field-derived estimates are based on direct dating of garnet using the apparent age difference between core and rim. The age data in these studies were obtained using two different approaches: (1) Garnet strongly prefers the parent (U, Sm) over the daughter (Pb, Nd) element and eventually develops radiogenic isotopic compositions of Pb and Nd. The fundamental assumption for dating is that the isotopic composition of the initially present daughter element was the same throughout garnet growth (e.g., Mezger 1989b; Vance and O'Nions 1990; Burton and O'Nions 1991; Burton et al. 1995). If this assumption is not fulfilled, the derived ages are incorrect (see above). (2) Garnet strongly prefers the daughter (Sr) over the parent (Rb) element. The Sr isotopic composition of garnet does not evolve after crystallization. The change in Sr isotopic composition reflects the evolution of Sr in the matrix, that is in the precursor minerals, during the time of garnet growth. The fundamental assumption of this approach is that the matrix is isotopically homogenous during garnet growth (e.g., Christensen et al. 1989, 1994). This assumption is only fulfilled if the different reactants are consumed in constant proportion or if the Sr isotopic composition in the matrix is continuously homogenized. For different kinds and changing proportions of reactants during garnet growth, the isotopic composition of Sr available for incorporation in garnet may have a variable isotopic composition and may not be represented by the Sr isotopic evolution of the bulk matrix. Our allanite–epidote data (Table 1; Fig. 2) show such heterogeneous initial $^{87}Sr/^{86}Sr$ due to the reaction history. Similarly, garnet from the Saxon granulites (sample 1/63–120/296 in Rötzler et al. (2004)) has initial $^{87}Sr/^{86}Sr$ values of 0.72228, whereas all other minerals from the same drill-core segment have values of 0.7091–0.7097 (unpublished

data). As the $^{87}Sr/^{86}Sr$ value of garnet is more radiogenic than the Sr composition of other major Sr-carrying phases, it cannot have been in isotopic equilibrium with the bulk matrix. Instead, it may be anomalously radiogenic because biotite, which had radiogenic $^{87}Sr/^{86}Sr$, was a precursor mineral. Thus, although intergranular transport and the availability of fluids may contribute to contrasting reaction rates by four to seven orders of magnitude in contact metamorphic aureoles and in regionally metamorphosed terranes (Baxter 2003), it is very likely that incorrect dating of mineral growth also contributed to this contrast.

Common to the above examples and explanations is that isotopic dating may yield incorrect estimates of geological rates, which eventually are used to model changes in material and heat transport or to calculate rates of deformation and reaction. Since age data from metamorphic minerals are widely used to unravel the *P–T–t–d*-evolution of orogens, inaccurate ages result in: (1) incorrect timing (duration) of *P–T*-loops and—consequently—erroneous rates of heat and mass transfer in orogens; (2) arbitrary rates (based on age difference between core and rim) for mineral growth, *P-T*-evolution, and deformation; and (3) an incorrect sequence of isotopic closure for the U–Pb systems in different minerals and a similarly incorrect sequence of isotopic closure of different isotope systems in the same mineral.

K_D—the ultimate control for anomalous initial isotopic signatures

The redistribution of elements from precursor minerals into different product minerals also transfers the isotopic signature of the precursors to the products. Such isotopic variability due to reaction history is well documented for stable isotope systems (Gregory and Criss 1986; Chamberlain et al. 1990; Kohn et al. 1993; Chamberlain and Conrad 1991, 1993; Young and Rumble 1993; Zheng et al. 2003). Although commonly ignored or thought to be insignificant, initial isotopic heterogeneity due to the reaction history also exists for radiogenic isotope systems (see examples above). The isotopic composition of the elements affected by radiogenic growth (e.g., Pb, Hf, Nd, Sr) depends on both the P/D ratio and the age of the precursor mineral. For minerals with a high P/D, the isotopic composition of Pb, Nd, and Sr being available during metamorphic reaction may be distinctly radiogenic. The incorporation of such radiogenic Pb, Nd, or Sr, which eventually may yield too old ages, is here referred to as chemical inheritance (cf. Romer 2001). Whether chemical inheritance occurs and yields anomalous ages depends on two controlling factors: (1) the K_D of the daughter element and (2) the nature of the precursor mineral.

(i) If the daughter element can be readily incorporated into the crystal lattice of the metamorphic mineral to be dated, the possibility of chemical inheritance exists. The amount of an initially incorporated daughter element depends on its availability and the distribution coefficient K_D: (1) between a reaction product and the precursor minerals and (2) among different reaction products. For instance, the incorporation of Pb in titanite may reach considerable levels when titanite is the only Ca-bearing mineral (Pb substitutes for Ca), but would be considerably lower, when titanite crystallizes together with calcite or Ca-rich feldspar. Furthermore, minerals with significant amounts of initial Pb have generally low $^{238}U/^{204}Pb$ values, which implies that they will evolve to less radiogenic $^{206}Pb/^{204}Pb$ and $^{207}Pb/^{204}Pb$ values than minerals with high $^{238}U/^{204}Pb$. Thus, initial isotopic heterogeneity in minerals that can incorporate larger amounts of Pb may become significant in comparison to in situ growth of radiogenic Pb. Our allanite–epidote sample illustrates this point in an extreme way, as the initial range in Pb isotopic composition (0.496 $^{206}Pb/^{204}Pb$ units) encompasses a larger range than in situ Pb growth over the last 240 Ma (0.364 $^{206}Pb/^{204}Pb$ units for the sample with the highest $^{238}U/^{204}Pb$). In contrast, minerals that have a small K_D for the daughter element (e.g., zircon, baddeleyite, rutile, columbite–tantalite–tapiolite) are typically insensitive to chemical inheritance.

(ii) The nature of the precursor minerals determines whether the initially incorporated daughter elements (e.g., Pb, Nd, Sr) show a large or small range in isotopic compositions or are homogeneous. The P/D value of the precursor mineral is here the controlling parameter. Extreme P/D ratios are obtained for phases that strongly enrich the parent element or that exclude the daughter element. Minerals with high P/D eventually develop anomalously radiogenic daughter isotope compositions, and their break-down during metamorphism makes the daughter elements available for incorporation into the reaction product. For instance, radiogenic Pb becomes available during the break-down of zircon, monazite, xenotime, rutile, or ilmenite. Radiogenic Sr is released during the decomposition of biotite and muscovite and radiogenic Nd is released during the consumption of garnet and xenotime. Thus, metamorphic reaction products that include one or several precursor minerals with high P/D may incorporate initial Pb, Nd, or Sr that is very different from Pb, Nd, or Sr of other metamorphic minerals. This contrast may eventually result in too old ages in some minerals if all minerals are corrected with the same initial Pb, Nd, or Sr isotopic composition. Using minerals with radiogenic initial Pb, Nd, or Sr together with other minerals to define a common isochron also yields an incorrect age. Thus, the nature of the precursor phases is important for the initial state of the isotope system used for dating. For instance, titanite that derived its Ti dominantly from the consumption of ilmenite or rutile may yield a too old age due to significant chemical inheritance (e.g., Romer and Rötzler 2003), whereas titanite that derived its Ti from biotite, amphibole, or pyroxene is unlikely to inherit isotopically anomalous Pb. As titanite that derived its Ti from rutile or ilmenite most likely has higher Nb contents than ti-

tanite that grew at the expense of biotite, amphibole, or pyroxene, the trace-element signature of the reaction product may provide a fingerprint for the precursor minerals. Analogous to titanite, allanite that formed at the expense of monazite is likely to have a markedly more radiogenic initial Pb isotopic composition than allanite that formed at the expense of zoisite.

Summary

A single allanite–epidote crystal that formed during UHP metamorphism of the Sulu belt (eastern China) shows heterogeneous initial Pb, Nd, and Sr isotopic compositions. Allanite–epidote probably formed between 250 and 220 Ma and records growth of both prograde allanite and retrograde epidote. Since most fragments had very low $^{238}U/^{204}Pb$, $^{232}Th/^{204}Pb$, and $^{87}Rb/^{86}Sr$ values, the initial heterogeneity has been preserved. The isotopic variation in the allanite–epidote crystal cannot be explained by the evolution of matrix Pb and Sr in the time span between the growth of the early allanite and the late epidote. Instead, the initial isotopic heterogeneity reflects changes in the precursor assemblage. The initial isotopic heterogeneity in allanite–epidote also implies that there was no isotopic homogenization among the precursor minerals.

The allanite–epidote crystal possibly formed during the prograde decomposition of zoisite. The elements Th, U, Nd, and Sm that are strongly fractionated into allanite are rapidly depleted in the zoisite source and their subsequent incorporation into epidote is controlled by other precursor silicates. The strong enrichment of LREE in allanite resulted in a relative enrichment of HREE in the precursor minerals, a signature that eventually is inherited in late epidote. The availability of Sr is originally dominated by zoisite and, thus, close to the composition of zoisite. More radiogenic initial Sr in epidote is observed only after zoisite had been consumed and other Sr sources significantly contributed to the Sr budget. The systematic shift of initial Pb isotopic composition from allanite to epidote suggests that the availability of Pb was never dominated by one phase alone.

Acknowledgments We thank Sten Littmann for purification and documentation of the individual allanite and epidote fragments and Cathrin Schulz for help with the chemical preparation of the samples. Much appreciated were constructive and detailed reviews by Felix Oberli (ETH Zürich) and Fernando Corfu (Olso). Y.X. gratefully acknowledges support from Deutsche Forschungsgemeinschaft through DFG-grant HO 375/22 and from the National Science Foundation of China.

References

Ames L, Tilton GR, Zhou G (1993) Timing of collision of the Sino-Korean and Yangtze cratons: U–Pb zircon dating of coesite-bearing eclogites. Geology 21:339–342

Anczkiewicz R, Thirlwall MF (2003) Improving precision of Sm–Nd garnet dating by H_2SO_4 leaching: a simple solution to the phosphate inclusion problem. In: Vance D, Müller W, Villa IM (eds) Geochronology: linking the isotopic record with petrology and textures. Geol Soc, London, Spec Publ vol 220, pp 83–91

Barr TD, Dahlen FA (1989) Brittle frictional mountain building 2. Thermal structure and heat budget. J Geophys Res 94:3923–3947

Barth S, Oberli F, Meier M (1989) U–Th–Pb systematics of morphologically characterized zircon and allanite: a high-resolution isotopic study of the Alpine Rensen pluton (northern Italy). Earth Planet Sci Lett 95:235–254

Barth S, Oberli F, Meier M (1994) Th–Pb versus U–Pb isotope systematics in allanite from co-genetic rhyolite and granodiorite: implications for geochronology. Earth Planet Sci Lett 124:149–159

Baxter EF (2003) Natural constraints on metamorphic reaction rates. In: Vance D, Müller W, Villa IM (eds) Geochronology: linking the isotopic record with petrology and textures. Geol Soc, London, Spec Publ vol 220, pp 183–202

Bea F (1996) Residence of REE, Th and U in granites and crustal protoliths; implications for the chemistry of crustal melts. J Petrol 37:521–552

von Blanckenburg F (1992) Combined high-precision chronometry and geochemical tracing using accessory minerals: applied to the Central-Alpine Bergell intrusion (central Europe). Chem Geol 100:19–40

Burton KW, O'Nions RK (1991) High-resolution garnet chronometry and the rates of metamorphic processes. Earth Planet Sci Lett 107:649–671

Burton KW, Kohn MJ, Cohen AS, O'Nions RK (1995) The relative diffusion of Pb, Nd, Sr and O in garnet. Earth Planet Sci Lett 133:199–211

Chamberlain CP, Conrad ME (1991) Oxygen-isotope zoning in garnet. Science 254:403–406

Chamberlain CP, Conrad ME (1993) Oxygen-isotope zoning in garnet: A record of volatile transport. Geochim Cosmochim Acta 57:2613–2629

Chamberlain CP, Ferry JM, Rumble D (1990) The effect of net-transfer reactions on the isotopic composition of minerals. Contrib Mineral Petrol 105:322–336

Christensen JN, Rosenfeld JL, DePaolo DJ (1989) Rates of tectonometamorphic processes from rubidium and strontium isotopes in garnet. Science 244:1465–1469

Christensen JN, Selverstone J, Rosenfeld JL, DePaolo DJ (1994) Correlation by Rb–Sr geochronology of garnet growth histories from different structural levels within the Tauern window, Eastern Alps. Contrib Mineral Petrol 118:1–12

Dahlen FA, Barr TD (1989) Brittle frictional mountain building 1. Deformation and mechanical energy budget. J Geophys Res 94:3906–3922

DeWolf CP, Zeissler CJ, Halliday AN, Mezger K, Essene EJ (1996) The role of inclusions in U–Pb and Sm–Nd garnet geochronology: stepwise dissolution experiments and trace uranium mapping by fission track analysis. Geochim Cosmochim Acta 60:121–134

Duchène S, Lardeaux J-M, Albarède F (1997) Exhumation of eclogites: insights from depth-time path analysis. Tectonophysics 280:125–140

Erambert M, Austrheim H (1993) The effect of fluid and deformation on zoning and inclusion patterns in poly-metamorphic garnets. Contrib Mineral Petrol 115:204–214

Faure G (1986) Principles of isotope geology, 2nd edn. Wiley, Chichester, pp589

Finger F, Broska I, Roberts MP, Schermaier A (1998) Replacement of primary monazite by apatite–allanite–epidote coronas in an amphibolite facies granite gneiss from the eastern Alps. Am Mineral 83:248–258

Franz L, Romer RL, Klemd R, Schmid R, Oberhänsli R, Wagner T, Dong Shuwen (2001) Eclogite-facies quartz veins within metabasites of the Dabie Shan (eastern China): pressure–

temperature–time-deformation-path, composition of the fluid phase and fluid flow during exhumation of high-pressure rocks. Contrib Mineral Petrol 141:322–346
Frei R, Biino GG, Prospert C (1995) Dating a Variscan pressure-temperature loop with straurolite. Geology 23:1095–1098
Frei R, Villa IM, Nägler TF, Kramers JD, Przybylowicz WJ, Prozesky VM, Hofman BA, Kamber BS (1997) Single mineral dating by the Pb–Pb step-leaching method: assessing the mechanisms. Geochim Cosmochim Acta 61:393–414
Frei D, Liebscher A, Franz G, Dulski P (2004) Trace element geochemistry of epidote minerals. In: Liebscher A, Franz G (eds) Epidotes. Rev Mineral Geochem vol 56, pp553–605
Frost BR, Chamberlain KR, Schumacher JC (2001) Sphene (titanite); phase relations and role as a geochronometer. Chem Geol 172:131–148
Gieré R, Sorensen SS (2004) Allanite and other REE-rich epidote-group minerals. In: Liebscher A, Franz G (eds) Epidotes. Rev Mineral Geochem vol 56, pp431–493
Glodny J, Austrheim H, Molina JF, Rusin AI, Seward D (2003) Rb/Sr record of fluid–rock interaction in eclogites: the Marun–Keu complex, Polar Urals, Russia. Geochim Cosmochim Acta 67:4353–4371
Grapes R, Bucher K, Hoskin P (2002) Monazite breakdown during amphibolite grade metamorphism: corona development and element diffusion. Eur J Mineral 14(Beiheft 1):58
Gregory RT, Criss RE (1986) Isotopic exchange in open and closed systems. In: Valley JW, Tylor HP Jr, O'Neil JR (eds) Stable isotopes in high temperature geological processes. Rev Mineral vol 16, pp91–127
Gromet P, Silver LT (1983) Rare earth element distributions among minerals in a granodiorite and their petrogenetic implications. Geochim Cosmochim Acta 47:925–939
Hermann J (2002) Allanite: thorium and light rare earth element carrier in subducted crust. Chem Geol 192:289–306
Humphries FJ, Cliff RA (1982) Sm–Nd dating and cooling history of the Scourian granulites, Sutherland, NW Scotland. Nature 295:515–517
Jaffey AH, Flynn KF, Glendenin LE, Bentley WC, Essling AM (1971) Precision measurement of half-lives and specific activities of ^{235}U and ^{238}U. Phys Rev C4:1889–1906
Jagoutz E (1995) Isotopic constraints on garnet equilibration. Terra Abstr 7(1):339
Johansson L, Lindh A, Möller C (1991) Late Sveconorwegian (Grenville) high-pressure granulite facies metamorphism in southwest Sweden. J Metam Geol 9:283–292
Kamber BS, Kramers JD, Napier R, Cliff RA, Rollinson HR (1995) The Triangle Shearzone, Zimbabwe, revisited: new data document an important event at 2.0 Ga in the Limpopo Belt. Precambr Res 70:191–213
Kohn MJ, Valley JW, Elsenheimer D, Spicuzza M (1993) Oxygen isotope zoning in garnet and staurolite: Evidence for closed system mineral growth during regional metamorphism. Am Mineral 78:988–1001
Kramers JD, Chavagnac V, Villa I (1999) Inclusions and the role of trace element partitioning in the retentivity of mineral chronometers during metamorphism. J Conf Abstr 4:712
Kühn A, Glodny J, Iden K, Austrheim H (2000) Retention of Precambrian Rb/Sr phlogopite ages through Caledonian eclogite facies metamorphism, Bergen Arc Complex, W-Norway. Lithos 51:305–330
Lanzirotti A, Hanson GN (1995) U–Pb dating of major and accessory minerals formed during metamorphism and deformation of metapelites. Geochim Cosmochim Acta 59:2513–2526
Le Roux JL, Glendenin LE (1963) Half-life of 232Th. Proc Natl Meet Nuclear Ener. Pretoria, South Aftrica, pp 83–94
Li SG, Xiao YL, Liu DL, Chen YZ, Ge NG, Zhang ZQ, Sun SS, Cong BL, Zhang RY, Hart SR, Wang SS (1993) Collision of the North China and Yangtze blocks and formation of coesite-bearing eclogites: timing and processes. Chem Geol 109:89–111
Li SG, Jagoutz E, Chen YZ, Li QL (2000) Sm–Nd and Rb–Sr isotopic chronology and cooling history of UHP metamorphic rocks and their country rocks at Shuanghe in the Dabie Mountains, Central China. Geochim Cosmochim Acta 64:1077–1093
Li SG, Huang F, Zhou HY, Li HM (2003) U–Pb isotopic compositions of the ultrahigh pressure metamorphic (UHPM) rocks from Shuanghe and gneisses from Northern Dabie zone in the Dabie Mountains, central China: Constraint on the exhumation mechanism of UHPM rocks. Science in China (D) 46(3):200–209
Liu FL, Xu ZQ, Liou JG, Katayama I, Masago H, Maruyama S, Yang JS (2002) Ultrahigh-pressure mineral inclusions in zircons from gneissic core samples of the Chinese Continental Scientific Drilling site in eastern China. Eur J Mineral 14:499–512
Liu FL, Xu ZQ, Liou JG, Song B (2004) SHRIMP U–Pb ages of ultrahigh-pressure and retrograde metamorphism of gneisses, south-western Sulu terrane, eastern China. J Metam Geol 22:315–326
Mezger K, Hanson GN, Bohlen SR (1989a) High-precision U–Pb ages of metamorphic rutile: application to the cooling history of high-grade terranes. Earth Planet Sci Lett 96: 106–118
Mezger K, Hanson GN, Bohlen SR (1989b) U–Pb systematics of garnet: dating the growth of garnet in the Late Archean Pikwitonei granulite domain at Cauchon and Natawuhunan Lake, Manitoba, Canada. Contrib Mineral Petrol 101:136–148
Mezger K, Essene EJ, Halliday AN (1992) Closure temperatures of the Sm–Nd system in metamorphic garnets. Earth planet Sci Lett 113:397–409
Möller A, O'Brien PJ, Kennedy A, Kröner A (2003) Linking growth episodes of zircon and metamorphic textures to zircon chemistry: an example from the ultrahigh-temperature granulites of Rogaland (SW Norway). In: Vance D, Müller W, Villa IM (eds) Geochronology: Linking the isotopic record with petrology and textures. Geol Soc, London, Spec Publ vol 220, pp65–81
Nagasaki A, Enami M(1998) Sr-bearing zoisite and epidote in ultra-high pressure (UHP) metamorphic rocks from the Su-Lu province, eastern China: An important Sr reservoir under UHP conditions. Am Mineral 83:240–247
Nyström AI, Kriegsman LM (2003) Prograde and retrograde reactions, garnet zoning patterns, and accessory phase behaviour in SW Finland migmatites, with implications for geochronology. In: Vance D, Müller W, Villa IM (eds) Geochronology: Linking the isotopic record with petrology and textures. Geol Soc, London, Spec Publ, vol 220, pp 213–230
Oberli F, Meier M, Berger A, Rosenberg CL, Gieré R (2004) U–Th–Pb and $^{230}Th/^{238}U$ disequilibrium isotope systematics. Precise accessory mineral chronology and melt evolution tracing in the Alpine Bergell intrusion. Geochim Cosmochim Acta 68:2543–2560
O'Brien PJ (1997) Garnet zoning and reaction textures in overprinted eclogites, Bohemian Massif, European Variscides: a record of their thermal history during exhumation. Lithos 41:119–133
Okay AI, Xu ST, Sengor AMC (1989) Coesite from the Dabieshan eclogite, central China. Eur J Mineral 1:595–598
Page L, Möller C, Johansson L (1996) 40Ar/39Ar geochronology across the Mylonite Zone and the Southwestern Granulite Province in the Sveconorwegian orogen of S. Sweden. Precambr Res 79:239–259
Parrish RR (2001) The response of mineral chronometers to metamorphism and deformation in orogenic belts. In: Miller JA, Holdsworth RE, Buick IS, Hand M (eds) Continental reactivation and reworking. Geol Soc, London, Spec Publ vol 184, pp289–301
Poitrasson F (2002) In situ investigation of allanite hydrothermal alteration: examples from calc-alkaline and anorogenic granites of Corsica (southeast France). Contrib Mineral Petrol 142:485–500
Romer RL (1992) Vesuvianite—a new tool for the U–Pb dating of skarn ore deposits. Mineral Petrol 46:331–341

Romer RL (2001) Lead incorporation during crystal growth and the misinterpretation of geochronological data from low-$^{238}U/^{204}Pb$ metamorphic minerals. Terra Nova 13:258–263
Romer RL, Nisca DH (1995): Svecofennian crustal deformation of the Baltic Shield and U–Pb age of late-kinematic tonalitic intrusions in the Burträsk Shear Zone, northern Sweden. Precambr Res 75:17–29
Romer RL, Rötzler J (2001) P–T–t evolution of ultrahigh-temperature granulites from the Saxon Granulite Massif, Germany. Part II: Geochronology. J Petrol 24:2015–2032
Romer RL, Rötzler J (2003) Effect of metamorphic reaction history on the U–Pb dating of titanite. In: Vance D, Müller W, Villa IM (eds) Geochronology: Linking the isotopic record with petrology and textures. Geol Soc, London, Spec Publ vol 220, pp147–158
Romer RL, Siegesmund S (2003) Why allanite may swindle about its true age. Contrib Mineral Petrol 146:297–307
Romer RL, Smeds S-A(1996) U–Pb columbite ages of pegmatites from Sveconorwegian terranes in southwestern Sweden. Precambr Res 76:15–30
Romer RL, Wright JE (1993) Lead mobilization during tectonic reactivation of the western Baltic Shield. Geochim Cosmochim Acta 57:2555–2570
Romer RL, Förster H-J, Breitkreuz Ch (2001) Intracontinental extensional magmatism with a subduction fingerprint: the late Carboniferous Halle Volcanic Complex (Germany). Contrib Mineral Petrol 141:201–221
Romer RL, Heinrich W, Schröder-Smeibidl B, Meixner A, Fischer C-O, Schulz C (2004) Elemental dispersion and stable isotope fractionation during fluid-flow and fluid immiscibility in the Bufa del Diente aureole, NE Mexico: evidenced from radiographies and Li, B, Sr, Nd, and Pb isotope systematics. Contrib Mineral Petrol (submitted)
Rötzler J, Romer RL, Budzinski H, Oberhänsli R (2004) Ultrahigh-temperature granulites from Tirschheim, Saxon Granulite Massif, Germany: P–T–t path and geotectonic implications. Eur J Mineral 16:917–937
Rubatto D, Hermann J (2001) Exhumation as fast as subduction? Geology 29:3–6
Schärer U, Zhang L-S, Tapponier P (1994) Duration of strike-slip movements in large shear zones: The Red River belt, China. Earth Planet Sci Lett 126:379–397
Stacey JS, Kramers 1JD (1975) Approximation of terrestrial lead isotope evolution by a two-stage model. Earth Planet Sci Lett 26:207–221
Steiger RH, Jäger E (1977) Subcommission of geochronology: Convention on the use of decay constants in geo- and cosmochronology. Earth Planet Sci Lett 36:359–362
Stosch H-G, Lugmair GW (1990) Geochemistry and evolution of MORB-type eclogites from the Münchberg Massif, southern Germany. Earth Planet Sci Lett 99:230–249
Thoeni M (2002) Sm–Nd isotope systematics in garnet from different lithologies (Eastern Alps); age results, and an evaluation of potential problems for garnet Sm–Nd chronometry. Chem Geol 185:255–281
Tilton GR, Grünenfelder MH (1968) Sphene: uranium–lead ages. Science 159:1458–1461
Vance D, Harris N (1999) Timing of prograde metamorphism in the Zanskar Himalaya. Geology 27:395–398
Vance D, O'Nions RK (1990) Isotopic chronometry of zoned garnets: growth kinetics and metamorphic histories. Earth Planet Sci Lett 97:227–240
Vance D, O'Nions RK (1992) Prograde and retrograde thermal histories from the central Swiss Alps. Earth Planet Sci Lett 114:113–129
Vance D, Meier M, Oberli F (1998) The influence of high U–Th inclusions on the U–Th–Pb systematics of almandine–pyrope garnet: results of a combined bulk dissolution, stepwise-leaching, and SEM study. Geochim Cosmochim Acta 62:3527–3540
Villa IM (1998) Isotopic closure. Terra Nova 10:42–47
Wang XD, Söderlund U, Lindh A, Johansson L (1998) U–Pb and Sm–Nd dating of high-pressure granulite and upper amphibolite facies rocks from SW Sweden. Precambr Res 92:319–339
Whitehouse MJ (2003) Rare earth elements in zircon: a review of applications and case studies from the Outer Hebridean Lewisian Complex, NW Scotland. In: Vance D, Müller W, Villa IM (eds) Geochronology: Linking the isotopic record with petrology and textures. Geol Soc, London, Spec Publ vol 220, pp49–64
Xiao YL, Li SG, Jagoutz E, Chen W (1995) P–T–t path for coesite-bearing peridotite-eclogite association in the Bixiling, Dabie Mountains. Chin Sci Bull 40:156–158
Xiao YL, Hoefs J, van den Kerkhof A, Simon K, Fiebig J, Zheng YF (2002) Fluid evolution during HP and UHP metamorphism in Dabie Shan, China: Constraints from mineral chemistry, fluid inclusions and stable isotopes. J Petrol 43:1505–1527
Xu ST, Okay AI, Ji S, Sëngor AMC, Su W, Liu YC, Jiang LL (1992) Diamond from the Dabieshan metamorphic rocks and its implication for tectonic setting. Science 256:80–82
Xu QD, Ouyang JP, Zhang BR, Kuang SP (2002) Tectonic affinity of Paleozoic stratigraphic slices along the northern margin in Dabie Orogen, central China: evidence from Pb isotope of rocks. Prog Natl Sci 12:438–444
Young ED, Rumble D (1993) The origin of correlated variations in situ $^{18}O/^{16}O$ and elemental concentration in metamorphic garnet from southeastern Vermont, USA. Geochim Cosmochim Acta 59:2095–2104
Zartman RE, Doe BR (1981) Pumbotectonics—the model. Tectonophysics 75:135–162
Zhang RY, Liou JG (1998) Ultrahigh-pressure metamorphism of the Sulu Terrane, Eastern China: A prospective view. Continent Dynam 3:32–53
Zhang HF, Sun M (2002) Geochemistry of Mesozoic basalts and mafic dikes, southeastern North China craton, and tectonic implications. Int Geol Rev 44:370–382
Zheng Y-F, Zhao Z-F, Li S-G, Gong B (2003) Oxygen isotope equilibrium between ultrahigh-temperature metamorphic minerals and its constraints on Sm–Nd and Rb–Sr chronometers. In: Vance D, Müller W, Villa IM (eds) Geochronology: linking the isotopic record with petrology and textures. Geol Soc, London, Spec Publ vol 220, pp93–117
Zhou B, Hensen BJ (1995) Inherited Sm/Nd isotope components preserved in monazite inclusions within garnets in leucogneiss from East Antarctica and implications for closure temperature studies. Chem Geol 121:317–326